

Promising Biomass Derived Functional Carbon from *Brassica oleracea* (Leaf) for Super Capacitor Applications

R. KAVIYASHRI¹, S. MANIMEGALAI^{2,*}, C. DHIVYA¹, A. PRITHIBA^{1,*} and A. MATHINA³

¹Department of Chemistry, Avinashilingam Institute For Home Science and Higher Education for Women, Coimbatore-641043, India

²Post Graduate and Research Department of Chemistry, Arulmigu Palaniandavar College of Arts & Culture, Palani-624601, India

³Department of Science and Humanities, Sri Sai Ranganathan Engineering College, Coimbatore-641109, India

*Corresponding authors: E-mail: mani_megalai22@yahoo.in; prithipete@gmail.com

Received: 23 September 2023;

Accepted: 22 October 2023;

Published online: 2 December 2023;

AJC-21460

The progress in development of novel electrode materials is critical for invention of energy storage devices as increased energy consumption necessitates extremely effective energy conversion. The biomass material (waste) obtained from *Brassica oleracea* (Leaf) was successfully transformed into functional carbon for use as electrode materials in electrochemical applications. The samples BOL-800 and BOL-900 were characterized using FT-IR spectroscopy and elemental analysis, which indicated the presence of functional carbon. The XRD analysis confirmed the amorphous nature of the synthesized samples, whereas SEM images clearly confirmed the formation of micro-size pores. Thermogravimetric analysis of BOL-800 indicated the progression of gasification reaction. Specific capacitance values for samples BOL-800 and 900 were calculated using cyclic voltammetry and galvanostatic charge discharge at current density of 0.5 A/g. Among the tested electrodes, BOL-900 electrode was found to exhibit superior specific conductance.

Keywords: *Brassica oleracea* L., Biomass, Super capacitor, Functional carbon, Electrochemical measurements.

INTRODUCTION

Growing interest in furthering the development of electric devices as energy and power sources, as well as a backup for renewable sources has been sparked by the evacuation of the world's energy supply. Electrochemical capacitors, among other options, show promise for peak power supplies, load balancing and energy recovery. Cost reduction is a key component in the widespread commercialization of electrochemical capacitors [1]. The growth of reliable, effective and pollution-free energy sources is necessary to meet rising energy demand and address a pressing environmental and health issues. A new generation of environmentally friendly energy storage devices must be integrated into our current energy storage technology in order to mitigate the impacts of environmental unrest. An apparatus for storing and then releasing electrical energy is known as an energy storage device [2].

Super capacitor has become a revolutionary energy storage technology. They are also referred to as electrochemical dual layer capacitor (EDLC) and ultra capacitors. In a super capacitor,

the area per gram of electrode is thousands of square metres, while the distance between the electrodes is measured in angstroms (Å). Super capacitors combine the properties of capacitors and batteries into one device [3,4].

Energy storage in EDLCs depends solely on electrostatic forces to build up charge at electrodes [5], as opposed to traditional batteries' use of charge-transfer processes. Surface area has an impact on a carbon electrode material's specific capacitance, although pore size distribution and the presence of functional groups also have a significant role. The impact of pore size on EDLC has been investigated recently. Pore size less than 0.5 nm and bigger than 2 nm are too wide for double-layer information in aqueous electrolytes [6]. Activated carbon is the component of modern super capacitors that is utilized the most frequently.

Recent developments in carbon super capacitor electrodes have seen the manufacture of activated carbon from waste biomass materials. Super capacitors made of biomass materials such seaweed biopolymers, used coffee grounds, fir wood, corn grains, banana fibres and sugar cane bagasse have been reported

[7]. These materials also make up super capacitors with carbon electrodes. The most recent developments in carbons generated from biomass for application in lithium-ion batteries, super capacitors, electrocatalytic water splitters and fuel cells.

In this research, the applicability of the biomass based carbon electrodes in super capacitor using cyclic voltammetry, impedance and galvanostatic charge discharge techniques from suitable ecological source *Brassica oleracea* L. (BOL) for the synthesis of functional carbon has been investigated.

EXPERIMENTAL

Synthesis of functional carbon from *Brassica oleracea*:

The present work focussed on the synthesis of hierarchical porous carbon materials using cauliflower leaves (*B. oleracea*) as a raw material. Large amounts of the dried and waste cauliflower leaves were gathered, carefully cleaned and dried in an oven at 60 °C. These dried BOL were preserved in a dry environment after being ground into fine ash. For the purpose of producing functional carbon, 10 g of dried BOL powder was heated in tube furnace for 3 h at 800 and 900 °C at a heating rate of 10 °C/min. Following a 5 mol/L HCl solution washing, the resulting black solid was dried for 12 h at 60 °C [8,9]. The BOL-800 and BOL-900 are the abbreviations for the freshly carbonized samples at these temperatures.

Characterization: The IR spectral (4500-400 cm⁻¹) analysis of powdered materials was conducted through Perkin-Elmer FT-IR spectrophotometer using SOFTWARE-OPUS version 6.5. The SEM images of the powdered materials was obtained from JEOL MODEL JSM 6360. The SEM analysis has been utilized particularly to assess structural changes in silicate particles following various thermal treatments and it is quite helpful to gain precise information about pore structure and surface morphology of functional carbon [10]. The structural analysis of BOL-800 and BOL-900 was ascertained using XRD. A thermobalance TGA/DSC 3+ from Mettler Toledo (USA) with a purge gas flow of 50 mL/min was used for analysis. The experiment was conducted with temperatures ranges 300 °C to 800 °C at heating rate of 30 °C/min.

Electrode fabrication: Initially, slurry of components was made by combining the binder (5 wt.% polyvinylidene difluoride dissolved in 1-methyl-1,2-pyrrolidinone (NMP)) and 85 wt.% BOL with 10 wt.% ketjen black in an agate mortar. The slurry was coated on toray carbon sheet of 1 cm² area and vacuum desiccated at 80 °C for an overnight period. A 1 M H₂SO₄ was employed as electrolyte in this study.

Electrochemical characterization: Electrochemical characterization was conducted out in a CH electrochemical workstation using a three-electrode system. Impedance dimension was approved out at frequency range of 100 kHz to 10 mHz with amplitude of 5 mV. The capacitance was calculated using:

$$C' = \frac{Z''}{2\pi f |Z|^2} \quad (1)$$

$$C'' = \frac{Z'}{2\pi f |Z|^2} \quad (2)$$

where f is frequency (Hz), Z' and Z'' are real and imaginary parts of impedance Z , respectively.

The potentials of cyclic voltammetry (CV) analysis were within range of 0.8 to -0.2 V and different scanning rates scan rates of 10-50 mV/s were used. Galvanostatic charge-discharge (GCD) examined were done at different current densities from 0.5 to 5 A/g, respectively. The gravimetric specific capacitance for a three-electrode system can be determined using the following formulae:

$$C = \frac{I \times \Delta t}{m \times \Delta V} \quad (3)$$

where I is discharge current (A), Δt is discharge time (s), ΔV is the voltage (V) and m is mass of active materials (g). The volumetric-capacitance is calculated by equation:

$$CV = C \times \rho \quad (4)$$

where ρ (g cm⁻³) is density of electrode materials. The energy density E (W h kg⁻¹) and the power density P (W kg⁻¹) are calculated by equations:

$$E = C \times \frac{\Delta V^2}{2 \times 4 \times 3.6} \quad (5)$$

$$P = \frac{3600E}{\Delta t} \quad (6)$$

RESULTS AND DISCUSSION

Characterization of functionalized carbon materials

FT-IR studies: Fine powder of crude BOL (Fig. 1a) confirmed the presence of C=O group corresponding to peak at 1614 cm⁻¹. The peaks at 2923 cm⁻¹ correspond to the C-H stretching vibrations, while an intense band at 1015 cm⁻¹ would be consigned to C-O stretching and C-C stretching vibrations [11,12]. Hence, it can be inferred that the crude BOL powder is abundant with oxygen comprising functional groups (O-H, C=O, C-O, C-C), aromatic ring, which encounters general structural consideration of functional carbons. An intense peak at 3735 cm⁻¹ observed in BOL 800 attributed to the O-H group of stretching vibration of H₂O molecule was found to diminish in BOL-900 sample. A long and sharp absorption peak at 2352 cm⁻¹ owed to the stretching vibration of C≡C alkyne. Peak pertaining to 1741 cm⁻¹ might be owing to -C=O stretching vibrations of esters. The bands between 675 and 1000 cm⁻¹ may be attributed to C-H stretching vibration, while a peak at 690 cm⁻¹ demonstrated a presence of aromatic C-H bending vibration in samples. In BOL-900 sample, the intensities at 3700-3000 and 1450-1000 cm⁻¹ are attributed due to the weakened the hydroxyl group bands, while a new-fangled vibration band of =C-O-C groups appeared at 1212 cm⁻¹ may be attributable to desiccation reactions. Similarly, a strong peak at 2343 cm⁻¹ may be ascribed to C≡C alkyne, while the penetrating band at 1732 cm⁻¹ displays the C=O stretching vibrations of esters.

Thermal studies: According to the current findings, the pyrolytic reaction of organic molecules entails the breaking of chemical bonds with temperature and the re-polymerization

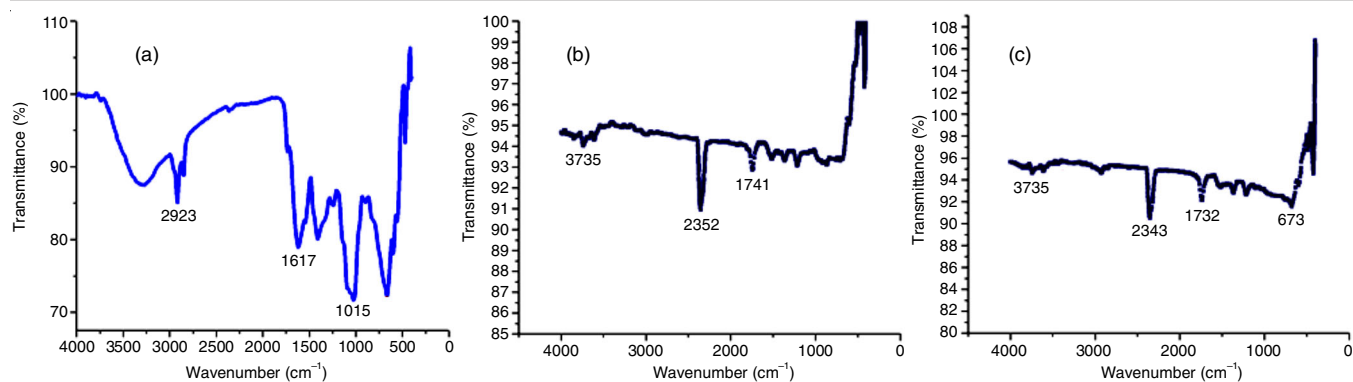


Fig. 1. FT-IR spectral peaks of (a) crude BOL, (b) BOL-800 and (c) BOL-900

of radicals that subsequently condense into active chemicals. During the carbonization, these chemicals produced the usual graphitic layers and planar stakes [13]. The BOL samples when subjected to TGA analysis decompose rapidly below 100 °C which may be attributed to the presence of adsorbed water molecules. The phenomenon of stark reduction was found to occur within the temperature range of 100-190 °C, which could be due to pyrolysis of oxygen comprising functional groups which yields CO, CO₂ and steam [14]. Due to lignin's tendency to decompose at higher temperatures, the TG curve has a tendency to flatten. More volatile chemicals were released as the temperature increase and thus lowering char yields [15].

TGA profile of BOL-800 and BOL-900 exhibited weight loss around 23.1% and 22.2%, respectively. All DTA curves for the investigated samples contained only one carbonaceous product reflects the exothermal reactions represented by a unique peak, as shown in Fig. 2. In the DTG curve, the peak height rises linearly as activation energy increases [16].

Morphological studies: The SEM images were used to explore the surface structure and the porosity of the BOL carbon materials prepared at 800 and 900 °C (Fig. 3). The production of thick and massive carbon particles for BOL-800 was visible in the SEM pictures, as illustrated in Fig. 3a. In this study, the SEM images of the BOL samples exhibited typical shapes as spherical and generally were random and non-uniform. Thus,

it may be said that oxygen-containing groups on surface of raw BOL have played critical role in formation of 3D hierarchical porous carbon.

The oxygen content of biomass carbon is high due to the presence of oxygen functional groups. The oxygen functional groups were removed during high-temperature pyrolysis and some pore canals were created on the surface, increasing the specific surface area of the resulting carbon spheres. The SEM images revealed the presence of carbon spheres that were aggregated and stacked. This observation suggests the occurrence of backbone development, which is associated with the local solid sintering process. Additionally, BOL-900 SEM images showed that the carbon particles were made up of network of carbon fibers that are crosslinked to form carbon spheres, which together form a 3D porous structure.

The EDS analysis of the BOL samples at BOL-800 and BOL-900 indicated that carbon percentage content was maximum as shown in Fig. 4. Due to the presence of potassium atoms in the biomass extract, the spectra exhibit additional lines that prove the presence of potassium (Table-1).

XRD analysis: Fig. 5 depicts the XRD patterns of BOL-800 and BOL-900. Two large peaks in BOL samples were seen at $2\theta = 25$ and 45 , which are reflective of (002) and (001), respectively. High porosity in the sample was also indicated by a clear rise in intensity at low-angle area of XRD pattern.

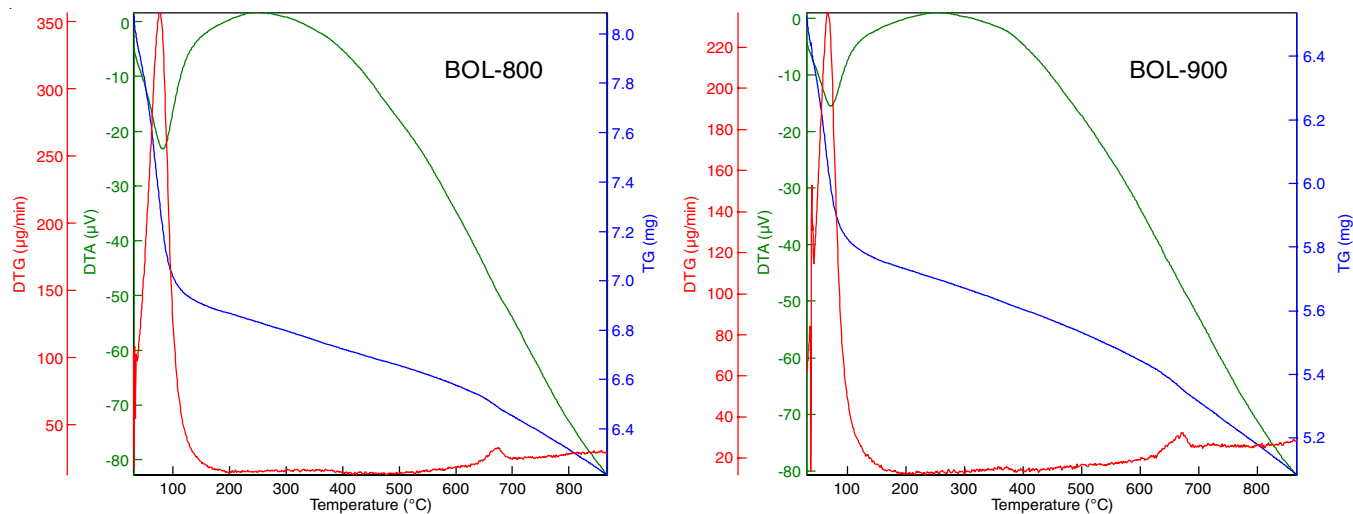


Fig. 2. TG-DTG and DTA of BOL-800 and BOL-900

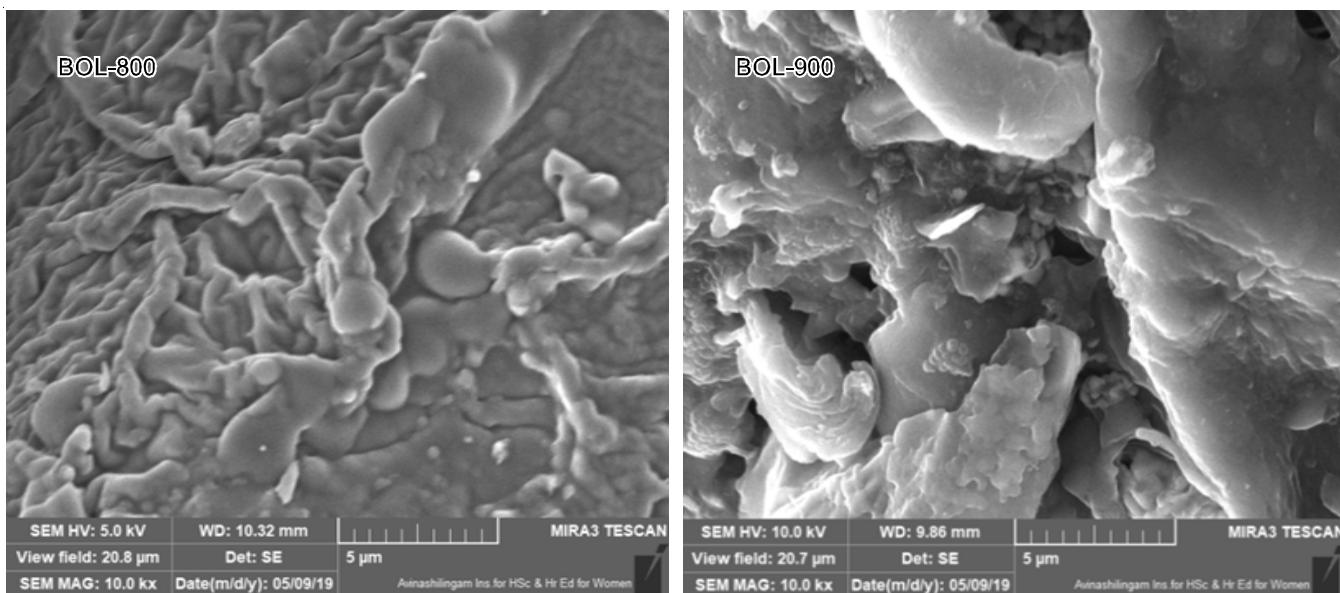


Fig. 3. SEM images of (a) BOL-800 and (b) BOL-900

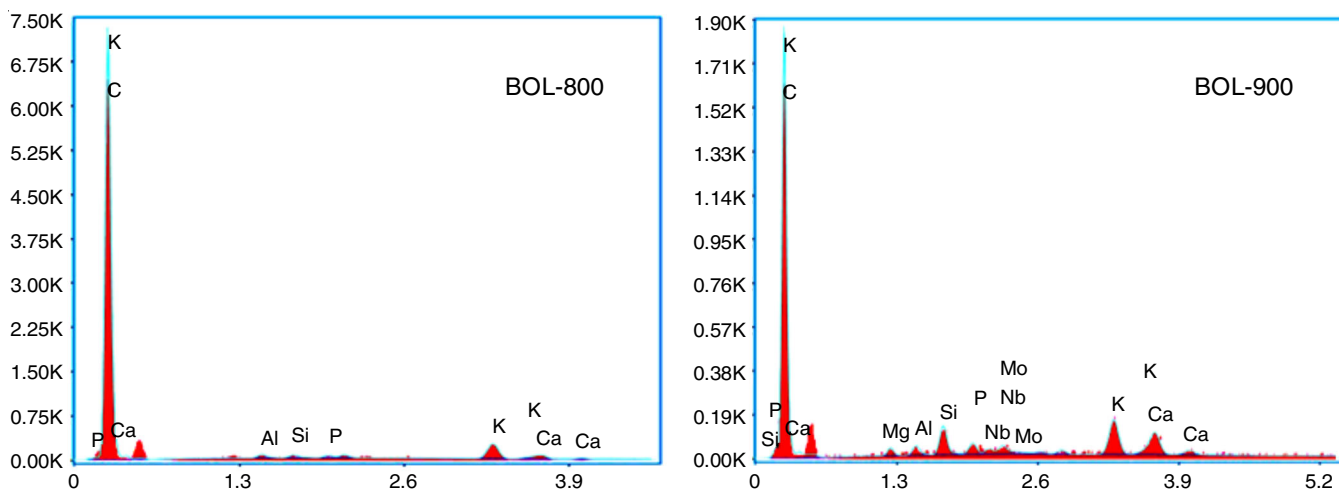


Fig. 4. EDS spectra of BOL-800 and BOL-900

Element	Atomic (wt.%)	
	BOL-800	BOL-900
C	97.56	93.44
O	—	—
Mg	—	0.41
Si	0.20	1.15
Zr	—	—
K	1.36	2.16
Ca	0.45	1.72
Al	0.24	0.41
P	0.19	0.49
Mo	—	0.23

Electrochemical measurements: The electrochemical response of fabricated electrodes BOL-800 and BOL-900 were measured in 1 M H₂SO₄. The active mass of BOL-800 and BOL-900 coated on toray carbon sheet was 0.88 mg and 0.81 mg, respectively.

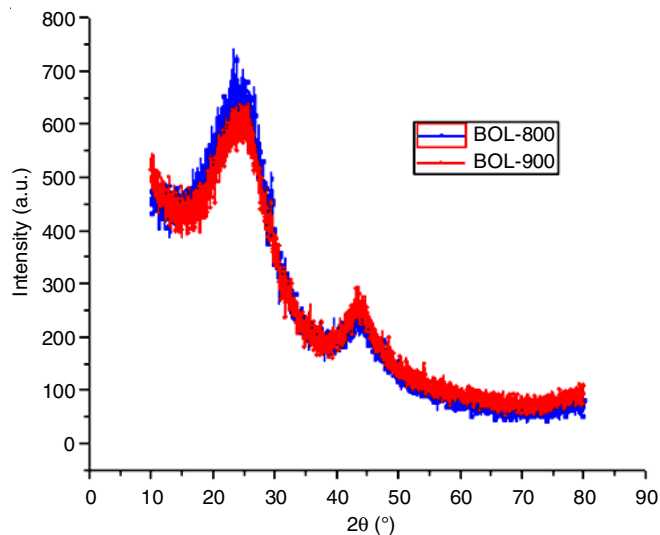


Fig. 5. XRD analysis of BOL-800 and BOL-900

Cyclic voltammetry studies: Cyclic voltammetry studies were conducted within a potential window range of 0-0.8 V, at various scan rates from 10 to 50 mV s⁻¹. The BOL-800 and BOL-900 samples reflected nearly rectangular-shaped CV patterns demonstrating their capacitive nature. The specific capacitance values obtained for BOL-800 at scan rates of 10, 20, 30, 40, 50 mV/S were 17, 16, 15.6, 15.4, 15.2 F/g, respectively (Fig. 6). The specific capacitance values obtained for BOL-900 at dissimilar scan rates of 10, 20, 30, 40, 50 mV s⁻¹ were 148.4, 140.49, 134.76, 129.63, 124.90 respectively. As scan rate increased, the capacitance decreased. The electrode material's resistivity, the output current at various potentials and the voltage drop all played a role in the whole process [17].

Galvanostatic charge-discharge: At current density of 0.7 A/g, charge/discharge curve displays an essentially triangular profile with slight interval resistance (IR) decrease, suggesting

high level of charge and discharge symmetry. Equivalent series resistance (ESR) phenomenon is typically linked to presence of an IR decrease at start of a discharge. The specific capacitances of BOLs from charge discharge studies at various current densities. Specific capacitance rapidly dropped with an increase in current density because the electrolyte did not have enough time to diffuse into all of the pores under the high current density.

Specific capacitances of BOL-800 and BOL-900 were 7.38 and 69 A/g, respectively (Fig. 7). The high specific surface area of the BOL-900 sample, which may provide increased contact area between electrode and electrolyte for buildup of ions, is primarily responsible for the exceptional capacitive performance of the device [18]. The energy density for BOL-900 sample was 1.38 W h Kg⁻¹.

Electrochemical impedance spectroscopic (EIS) studies: EIS was used to record interfacial characteristics of electrodes

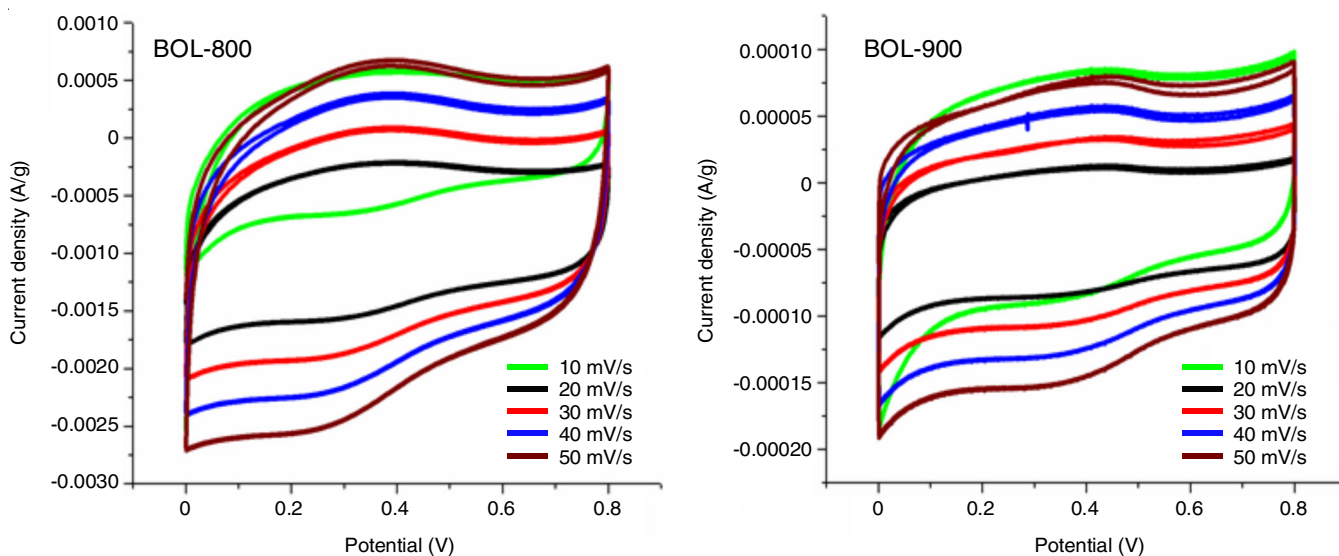


Fig. 6. Cyclic voltammetry curves of BOL-800 and BOL-900 and (d) Considered specific capacitance from CV curves at different scan rates and cyclic voltammetry curves of BOL electrodes

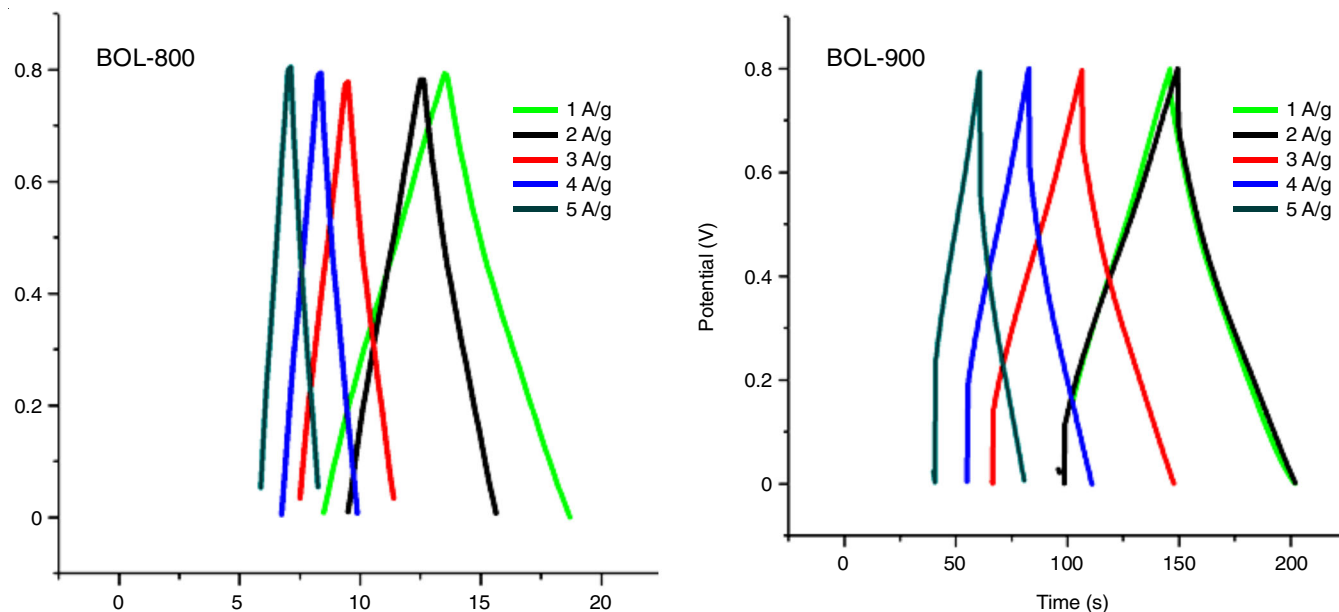


Fig. 7. Galvanostatic charge discharge of BOL-800 and BOL-900 and relationship between current density and specific capacitance

(BOL-800 and 900 samples) and the findings are shown in Fig. 8. An almost optimal capacitive behaviour for BOL-800 and BOL-900 electrode materials in 1 M H₂SO₄ solution is indicated by the Nyquist plot's vertical curve and low Faradic charge transfer resistance, which spans the frequency range of 10 KHz to 100 MHz. The BOL-900 system appears to have greater conductivity because the BOL-800 Nyquist plot showed smaller diameter of semicircular in the high frequency zone. At the same time, BOL-900 system's vertical form at lower frequencies pointed to an electrode that was acting more capacitively.

From Fig. 8a, it can be observed that in high to medium frequency range, the EDLC cell demonstrated capacitive behaviour as shown by a depressed semicircle in the impedance pattern. The carbonized spheres are not significantly altered by the activation process at 800 °C and the oxygen content of biomass carbon is high due to presence of oxygen functional groups. The oxygen functional groups are removed during high

temperature pyrolysis and some pore canals were developed on the surface, increasing the specific surface area (SSA) of the resulting carbon spheres.

In SEM images, stacked and aggregated carbon spheres are shown, which suggests that the neck formation connected to local solid sintering. This agglomeration reduced the surface area which decreased the capacitance of BOL-800 electrode system. The equivalent circuit used for analyzing the data is shown in inset of Fig. 8b. Here R1 is internal resistance, L1 inductance due to connection, R2 is charge transfer resistance and M is due to matter transport in thin layer in linear symmetry.

The contact area available between active electrode material and electrolytic solution may have the greatest impact on capacitance. To enable a successful charge transfer reaction, intimate communication between electrode and electrolyte must be made at same time [19]. In BOL-800, due to agglomeration of carbon spheres, the available contact area got decreased resulting in decreased capacitance as indicated in Table-2.

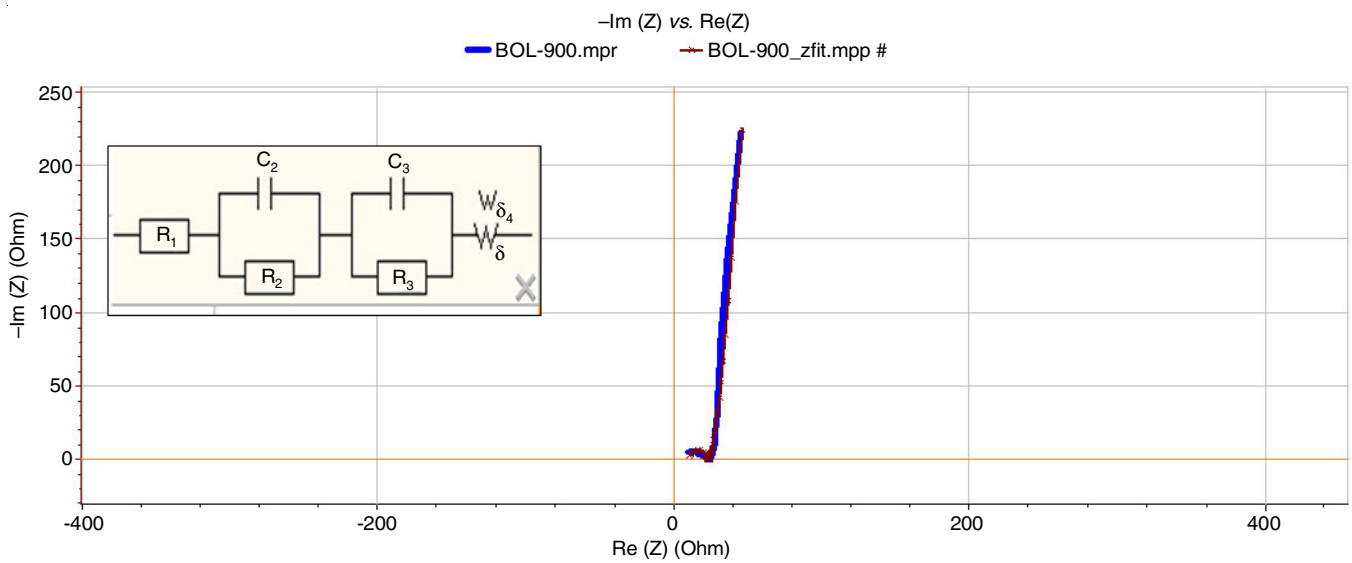


Fig. 8(a). Nyquist plot of BOL-900

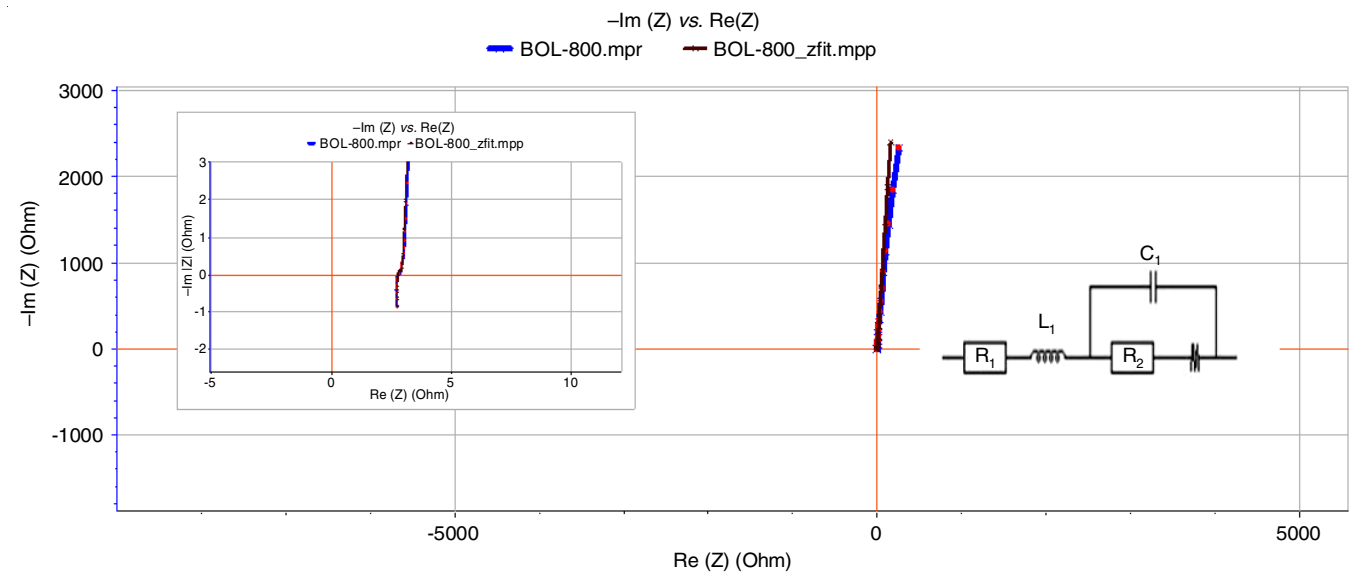


Fig. 8(b). Nyquist plot of BOL-800 based capacitors and equivalent circuit diagram

TABLE-2
AC IMPEDANCE FOR R_s AND CS

System	R _s (Ohms)	Sp. capacitance (F/g)
BOL-800	2.87	7.7
BOL-900	9.886	88

Conclusion

A study on electrochemical capacitors (ECs) as energy storage devices has been conducted in this work from an environmentally friendly perspective. Plant waste biomass material *Brassica oleracea* (L.) was procured and effectively synthesized into functional carbon to serve as ECs' electrode materials. Several analytical techniques were utilized for testing the synthesized functional carbon to ascertain indicated the possibility of utilizing these materials in energy sector. The samples BOL-800 and BOL-900 were characterized using FT-IR spectroscopy, which indicated the presence of functional carbon. XRD analysis confirmed the amorphous nature of the synthesized samples. TGA profile of BOL-800 around 23.1% and BOL-900 exhibited around 22.2% respectively. SEM images of BOL-800 and BOL-900 clearly confirm the formation of micro-size pores through the sample. Elemental analysis of BOL-800 indicated the progression of gasification reaction at 800 °C resulted in aggregated and stacked carbon spheres as observed in SEM image of BOL-800 that led to elimination of oxygen as observed in EDX results. BOL-800 contained a maximum carbon content of 97.56 atomic % while BOL-900 contained 93.44% of carbon content. From the results of cyclic voltammetry, the calculated specific capacitance values for BOL-800 and BOL-900 were 17.0 and 148.4 F/g, respectively. The results of GCD studies inferred a specific capacitance of 7.38 and 69 F/g for BOL-800 and BOL-900, respectively at current density of 0.5 A/g. The electrochemical studies indicated that BOL-800 and BOL-900 electrodes were adept of furnish specific capacitance of 7.8 and 88 F/g, respectively. Among the tested electrodes, BOL-900 electrode was found to exhibit superior specific conductance.

ACKNOWLEDGEMENTS

The authors are thankful to their respective Institutions for providing the necessary facility to carry out the study.

CONFLICT OF INTEREST

The authors declare that there is no conflict of interests regarding the publication of this article.

REFERENCES

- M. Sevilla, W. Gu, C. Falco, M.M. Titirici, A.B. Fuertes and G. Yushin, *J. Power Sources*, **267**, 26 (2014); <https://doi.org/10.1016/j.jpowsour.2014.05.046>
- E. Frackowiak and F. Beguin, *Carbon*, **39**, 937 (2001); [https://doi.org/10.1016/S0008-6223\(00\)00183-4](https://doi.org/10.1016/S0008-6223(00)00183-4)
- A.K. Shukla and S.K. Martha, *Resonance*, **6**, 52 (2001); <https://doi.org/10.1007/BF02835270>
- C. Lin, J.A. Ritter and B.N. Popov, *J. Electrochem. Soc.*, **146**, 3639 (1999); <https://doi.org/10.1149/1.1392526>
- A. Kumar, N. Kumar, P. Baredar and A. Shukla, *Renew. Sustain. Energy Rev.*, **45**, 530 (2015); <https://doi.org/10.1016/j.rser.2015.02.007>
- G. Gowri, K. Manimegalai and K. World, *J. Pharm. Pharm. Sci.*, **6**, 1277 (2017).
- S. Gao, Y. Chen, H. Fan, X. Wei, C. Hu, H. Luo and L. Qu, *J. Mater. Chem. A Mater. Energy Sustain.*, **2**, 3317 (2014); <https://doi.org/10.1039/c3ta14281g>
- T.E. Rufford, D. Hulicova-Jurcakova, E. Fiset, Z. Zhu and G.Q. Lu, *Electrochem. Commun.*, **11**, 974 (2009); <https://doi.org/10.1016/j.elecom.2009.02.038>
- S.G. Lee, K.H. Park, W.G. Shim, M.S. Balathanigaimani and H. Moon, *J. Ind. Eng. Chem.*, **17**, 450 (2011); <https://doi.org/10.1016/j.jiec.2010.10.025>
- B.Y. Yu and S.Y. Kwak, *J. Mater. Chem.*, **22**, 8345 (2012); <https://doi.org/10.1039/c2jm16931b>
- X. Zhu, S. Yu, K. Xu, Y. Zhang, L. Zhang, G. Lou, Y. Wu, E. Zhu, H. Chen, Z. Shen, B. Bao and S. Fu, *Chem. Eng. Sci.*, **181**, 36 (2018); <https://doi.org/10.1016/j.ces.2018.02.004>
- H. Chen, Y. Guo, F. Wang, G. Wang, P. Qi, X. Guo, B. Dai and F. Yu, *N. Carbon Mater.*, **32**, 592 (2017); [https://doi.org/10.1016/S1872-5805\(17\)60140-9](https://doi.org/10.1016/S1872-5805(17)60140-9)
- Q. Liang, L. Ye, Z.H. Huang, Q. Xu, Y. Bai, F. Kang and Q.H. Yang, *Nanoscale*, **6**, 13831 (2014); <https://doi.org/10.1039/C4NR04541F>
- X. Ma, C. Ding, D. Li, M. Wu and Y. Yu, *Cellulose*, **25**, 4743 (2018); <https://doi.org/10.1007/s10570-018-1903-3>
- N. Sudhan, K. Subramani, M. Karnan, N. Ilayaraja and M. Sathish, *Energy Fuels*, **31**, 977 (2017); <https://doi.org/10.1021/acs.energyfuels.6b01829>
- Z. Liu, Z. Zhu, J. Dai and Y. Yan, *ChemistrySelect*, **3**, 5726 (2018); <https://doi.org/10.1002/slct.201800609>
- H. Xuan, G. Lin, F. Wang, J. Liu, X. Dong and F. Xi, *J. Solid State Electrochem.*, **21**, 2241 (2017); <https://doi.org/10.1007/s10008-017-3562-y>
- R. Siddharthan, P. Mahalingam, E. Kanagaraj and K. Saravanan, *Asian J. Chem.*, **33**, 2621 (2021); <https://doi.org/10.14233/ajchem.2021.23346>
- K.K. Singh and A.K. Sharma, *Asian J. Chem.*, **32**, 1779 (2020); <https://doi.org/10.14233/ajchem.2020.22681>